

Red-giant collisions in the galactic centre

Vernon C. Bailey, Melvyn B. Davies[★]

Institute of Astronomy, Madingley Road, Cambridge CB3 OHA.

Received ** *** 1998; in original form 1998 *** **

ABSTRACT

We simulate collisions involving red-giant stars in the centre of our galaxy. Such encounters may explain the observed paucity of highly luminous red giants within ~ 0.2 pc of Sgr A*. The masses of the missing stars are likely to be in the range $\sim 2 M_{\odot} - 8 M_{\odot}$. Recent models of the galactic centre cluster's density distribution and velocity dispersion are used to calculate two-body collision rates. In particular we use stellar-evolution models to calculate the number of collisions a star will have during different evolutionary phases. We find that the number of two-body collisions per star is $\lesssim 1$ in the central 0.1 pc – 0.2 pc, depending strongly on the galactocentric radius, with some uncertainty from the assumed cluster models and stellar-evolution models. Using a 3D numerical hydrodynamics code (SPH) we simulate encounters involving cluster stars of various masses with a $2 M_{\odot}$ red giant and an $8 M_{\odot}$ red giant. The instantaneous mass loss in such collisions is rarely enough to destroy either giant. A fraction of the collisions do, however, lead to the formation of common envelope systems where the impactor and giant's core are enshrouded by the envelope of the giant. Such systems may evolve to expel the envelope, leaving a tight binary; the original giant is destroyed. The fraction of collisions that produce common envelope systems is sensitive to the local velocity dispersion and hence galactocentric radius. Whereas most of our collisions lead to common envelope formation at a few parsecs from Sgr A*, very few collisions do so within the central 0.2 pc. Using our collision-rate calculations we then compute the time-scales for a giant star to suffer such a collision within the galactic centre. These time-scales are $\gtrsim 10^{9-10}$ years and so are longer than the lifetimes of stars more-massive than $\sim 2 M_{\odot}$. Thus the observed paucity of luminous giants is unlikely to be due to the formation of common envelope systems as a result of two-body encounters involving giant stars.

Key words: stellar: collisions – Galaxy: centre – stellar dynamics

1 INTRODUCTION

Recent observations of the central stellar cluster of our galaxy reveal that the brightest K-giant stars ($2 - 8 M_{\odot}$ AGB stars or more-massive supergiants) are depleted within ~ 0.2 pc from Sgr A*, the dynamical centre of the Milky Way (Genzel *et al.* 1996). The missing stars are highly luminous and are therefore very large, and so Genzel *et al.* (1996) concluded that stellar collisions were a likely explanation for the paucity if the cluster's core density is sufficiently large to make collisions frequent and if such collisions permanently destroyed the photospheres of giants.

The effects of stellar collisions on giant stars have been previously investigated in the context of globular clusters

(Davies, Benz & Hills 1991; 1992). Such collisions often resulted in the impactor becoming bound to the giant's core within the envelope of the giant, forming a *common envelope* system. In such systems, the impactor and the core spiral towards each other and the binding energy released is deposited in the envelope which is ejected on time-scales shorter than the evolutionary time-scale of the giant. By this method the giant is destroyed, leaving behind a binary comprised of the impactor and the giant's core. Collisions in galactic centres differ from those in globular clusters due to the higher velocities involved. The higher velocity dispersions in galactic nuclei ($\sigma \gtrsim 100$ km/s) mean that incoming stars are faster and so are less likely to form bound systems than in globular cluster cores ($\sigma \sim 10$ km/s).

In this paper we investigate the frequency of two-body collisions involving main-sequence stars and also red giants. The red giants investigated are similar to those observed to

[★] Current Address: Department of Physics and Astronomy, University of Leicester, Leicester LE1 7RH

be depleted in the galactic centre (hereafter GC). We simulate a number of encounters involving the giants, quantifying the mass loss and probability of forming bound systems. If the GC contains binary stars, the collision time-scale between giants and binaries may be significant if the cluster density is sufficiently large. In a companion paper, Davies *et al.* (1998), we extend this study to collisions involving binary impactors.

In §2 we consider the stellar contents, motions and distribution within the central parsec of our galaxy, and we discuss the possible nature of the stars that currently cannot be detected. The stellar density profile and velocity dispersion are then used to calculate collision time-scales in §3. In §4 we consider how devastating an encounter must be to destroy a giant. We discuss our approach to simulating collisions involving red giants in §5 and we present our results in §6. In a number of collisions the impactor will become bound to the giant star. We comment on the nature of such systems in §7, prior to discussing our results in §8. Alternative methods of destruction for the giants are explored in §9. We summarise our findings in §10.

2 STELLAR CONTENTS, DISTRIBUTION & DYNAMICS OF THE CENTRAL PARSEC

2.1 Observable stars and the bright-giant paucity

Dust in the plane of our galaxy obscures the GC by ~ 30 magnitudes of visual extinction (Rieke, Rieke & Paul 1989). The infra-red K band ($2.2\ \mu\text{m}$) extinction is much less severe, $A_K \sim 3$ magnitudes (Rieke, Rieke & Paul 1989). The large distance to the GC ($\sim 8.5\ \text{kpc}$) gives a distance modulus of 14.6 which, coupled with $A_K \sim 3$, limits stellar observations to giant stars. Within the central $\sim 0.5\ \text{pc}$ of our galaxy there are ~ 600 red giants of magnitude $K \lesssim 15$ (Eckart *et al.* 1995). However, the brightest red giants are *not observed* in the deepest parts of the galactic nucleus. Observations show sharp drops in the numbers of $10.5 < K < 12$ stars at $\sim 0.12\ \text{pc}$ and of $K < 10.5$ stars at $\sim 0.2\ \text{pc}$ (Genzel *et al.* 1996). These highly luminous stars are unlikely to have been overlooked by observations. Indeed, the number counts in Genzel *et al.* (1996) of $10.5 < K < 12$ giants are likely to be 80–85% complete and the numbers of the $K < 10.5$ stars are 90–95% complete (Genzel, private communication). At slightly larger galactocentric radii, giants of similar luminosity to those missing have a surface-density profile, $\Sigma \propto p^{-1}$, for projected radius p . Assuming that this profile should extend further into the core, we estimate the numbers of missing giants to be twenty-five $K < 10.5$ magnitude stars and eleven $10.5 < K < 12$ magnitude stars. If the surface density were flat within the region of missing giants then lower limits of the numbers of missing $K < 10.5$ and $10.5 < K < 12$ giants are eleven and six respectively. We note that the *precipitous* drop, rather than a gradual one, indicates that some mechanism has actively destroyed at least $\sim 15 - 40$ stars in the central 0.2 pc.

2.2 The visible stellar population

The outcome of a collision between two stars will depend on their masses and sizes (*i.e.* evolutionary phases). It is

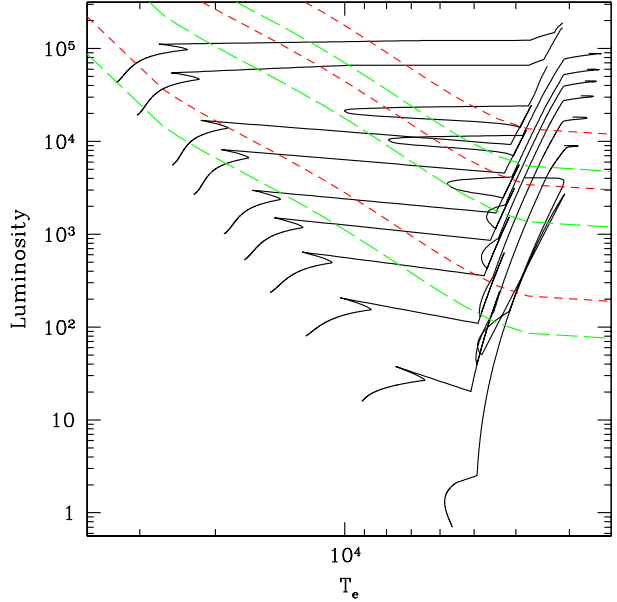


Figure 1. HR diagram showing theoretical evolutionary tracks for stars of masses 1, 2, 3, 4, 6, 8, 10, 15, $20\ M_{\odot}$, models based upon Pols *et al.* (1999) with metallicity $Z=0.02$. The full models include evolution from AGB tip to remnant; we have truncated the tracks at the AGB tip on this diagram for clarity. The long-dashed lines represent contours of K of 15, 12 and 10.5, based on $A_K = 3$ and a distance modulus of 14.6 to the GC; the short-dashed lines are the K contours of the same values but based upon $A_K = 4$. Effective temperature is in Kelvin, luminosity is solar.

useful to visualise the types of stars detectable (and those which are missing) at the GC using a HR diagram. For a star of given temperature and bolometric luminosity, its apparent K -magnitude may be calculated using bolometric corrections and V-K colours (Johnson 1966) and by assuming a distance modulus and a K -extinction law. Taking the galactocentric distance to be 8.5 kpc, Figure 1 shows a HR diagram with contours of constant K appropriate for the GC, assuming $A_K = 3$ and $A_K = 4$. The effects of uncertainties in the GC distance on the masses and numbers of stars one expects to see at the GC are small compared with uncertainties in A_K . Rieke, Rieke & Paul (1989) report $A_K = 2.7$; more recently Blum, Sellgren & DePoy (1996) have derived a mean K -extinction of 3.3 ± 0.9 but note that A_K may reach six in places. We see from Figure 1 that, for both values of A_K , the cool, visible stars must be giants and that we cannot easily determine their masses because of the closeness of the Hayashi tracks. The Figure does, however, imply that a visible low-mass star will likely be on the AGB phase, whilst for stars of increasing masses the horizontal branch becomes increasingly visible. The duration for which a star of a given K -magnitude is visible is an irregular function of its mass (Figure 2) depending on whether either the long-lived main-sequence or horizontal-branch phases coincide with the chosen K -magnitude. Figure 2 highlights the great sensitivity of the visible durations of stars on A_K . If $A_K = 3$, stars of mass $\lesssim 1.4\ M_{\odot}$ cannot be detected at $K < 10.5$. If $A_K = 4$, then stars of mass $\lesssim 2.5\ M_{\odot}$ cannot be detected at $K < 10.5$ and the time-scale for which the stars are visible falls sharply

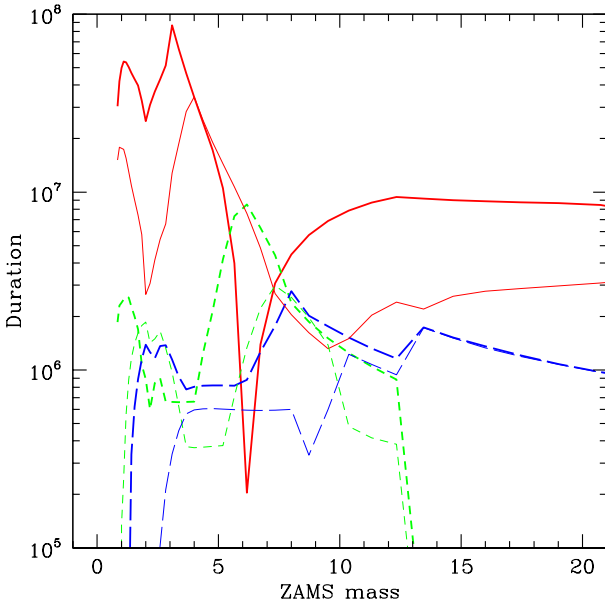


Figure 2. Visible time-scales for stars at the GC, based on stellar models as described in Figure 1. The solid line denotes the time-scale for which the star is visible as $15 < K < 12$, the short-dashed line represents the time-scale for which the star is visible as $12 < K < 10.5$ and the long-dashed line shows the visible duration in the $K < 10.5$ band. Heavy lines show the time-scales for $A_K = 3$; less bold lines represent $A_K = 4$. The “kinks” in the profiles can be attributed to different parts of the stars’ evolution (e.g. horizontal branch) overlapping with a given K-luminosity band. Note that stars of masses less than $\sim 0.9 M_\odot$ will not ascend the giant branch within a Hubble time.

for masses $< 4 M_\odot$. Assuming $A_K = 3$, stars of most masses are brighter than $K=10.5$ for about 10^6 years and most stars of magnitude $10.5 < K < 12$ are visible for $6 - 85 \times 10^5$ years. For stars of masses in the region of $6 M_\odot$, the horizontal branch shines in the $10.5 < K < 12$ band rather than in the $12 < K < 15$ band. We thus see a steep drop in the time that such stars spend in the fainter band, and a corresponding peak in the brighter band. The $10.5 < K < 12$ range corresponds to the Hertzsprung Gap for stars of higher masses and so the $10.5 < K < 12$ durations drop. The bulk of detectable stars sit in the $12 < K < 15$ bin in which low-mass stars are visible for $\sim 3 - 6 \times 10^7$ years (still assuming that $A_K = 3$); higher-mass stars are visible for 10^7 years. The fluctuation in visible duration for low-mass stars in the $12 < K < 15$ range is due to changes in positioning of the core-helium burning phase with respect to the $K = 15$ contour. Increasing A_K to four generally decreases the visible time-scales by a factor of a few (but within an order of magnitude). Some stars may have their visible time-scales boosted in some K-magnitude range because, say, their horizontal branches now correspond to a lower K-magnitude bin in which, for lower A_K , only part of their giant branches had been detectable.

2.3 The entire stellar population

The contours of constant K-magnitude on Figure 1 show that detectable stars must be either evolved stars of a range of masses or very massive stars if they are on the main sequence. If the GC population consists mainly of low-mass main-sequence stars and stellar remnants then we only glimpse a small fraction of the total mass of the GC stellar population. Indeed, the detectable stars’ motions and distribution have been used to measure the total mass in the central parsec to be $\sim 4.2 \times 10^6 M_\odot$, of which $2.5 \times 10^6 M_\odot$ is the mass of the putative supermassive black hole at the centre of the cluster (Genzel *et al.* 1996, Eckart & Genzel 1997). The amount of stellar mass in the central parsec is therefore about $1.7 \times 10^6 M_\odot$. We saw in §2.2 that only stars of masses $\gtrsim 1.4 M_\odot$ may be seen in the GC if $A_K = 3$. Assuming a Scalo IMF, stars of masses $> 1.4 M_\odot$ can account for about a quarter of the mass of the population, if the mass contribution from stellar remnants is small. Figure 2 shows that low-mass giants may be detectable for about 4×10^7 years, depending on the stellar mass. Given that a $1.4 M_\odot$ star lives for $\sim 4 \times 10^9$ years (Pols *et al.* 1999), for a constant star-formation rate one might expect to see ~ 3000 stars within the central parsec. This is about a factor of two higher than, but is not wildly inconsistent with, the number counts one would observe by extrapolating the observed numbers of stars within 0.5 pc (Eckart *et al.* 1995) out to a radius of 1 pc .

A more detailed population synthesis was performed by Genzel *et al.* (1994); they found that the GC stellar contents were inconsistent with a constant star-formation history and Salpeter IMF. Detailed analyses are, however, hampered by uncertainties in A_K , possible incompleteness in the observed number counts and that there may not be a unique solution of IMF or star-formation history (or of both) which reproduces the observations.

The situation is even further complicated by the possibility of a raised low-mass cut-off to star formation at the GC (Morris 1993). For a cut-off of $\sim 0.8 M_\odot$ and a constant star-formation history, one might expect roughly equal numbers of white dwarfs and main-sequence stars. Higher low-mass cut-offs may allow stellar remnants to dominate the population, assuming that the population is old. A further complication is that the GC stellar contents may not be totally indigenous. Morris (1993) calculates the mass fractions of neutron stars and black holes that may have segregated into the central parsec from outside. Solutions computed by Morris (1993) allow most of the GC mass to be accounted for by black holes and neutron stars. These calculations, however, suffer from requiring some parameters that are not well constrained, such as the low-mass cut-off and the mass of stellar black holes. For example, lowering the mass of stellar black holes from $10 M_\odot$ to $3 M_\odot$ and adopting a low-mass cut-off of $0.08 M_\odot$ reduces the mass-fraction of neutron stars and stellar-mass black holes to $< 10\%$ by mass. There will almost certainly be non-indigenous remnants in the GC, but in quantities which are currently poorly constrained.

The overall mass function of the GC population is therefore very uncertain. For $A_K = 3$, we might expect most of the missing giants to be of low masses (say, $1.4 M_\odot - 3 M_\odot$), for most IMFs. However, the uncertainty in A_K could mean that the brightest missing stars are of masses $\gtrsim 4 M_\odot$.

2.4 Distribution and motions of GC stars

An observed number density of stars traces that of the whole cluster if the mean mass of the cluster stars is close to the mean mass of the observed stars and if the system is relaxed. The relaxation time (see Binney & Tremaine 1987) at 0.2 pc is $\sim 2 \times 10^9$ years for a $1 M_\odot$ star, so we expect low-mass ($1 - 2 M_\odot$) giants to trace the overall distribution of stars of similar masses. Relaxation time decreases with the mass of the star but more-massive stars do not live long enough to become relaxed in the GC. Such stars should be treated cautiously as mass tracers. Genzel *et al.* (1996) model the observed red-giant number-density distribution to be

$$n(r) \propto \left(\frac{1}{1 + (r/4.2'')^{1.8}} \right) \quad (1)$$

for galactocentric radius, r . We adopt this Equation, assuming that the observed stars are indeed tracing the whole population. This assumption is somewhat supported by the stars' isotropic motions (Genzel *et al.* 1996, Eckart & Genzel 1997), indicating a relaxed population. Genzel *et al.* (1996) also give the central stellar density, ρ_0 , to be $4 \times 10^6 M_\odot/\text{pc}^3$ and a core radius of 0.38 pc. We normalise Equation (1) with this value of ρ_0 but note that ρ_0 and the core radius are inter-linked values and that the latter is subject to some debate, depending on whether the cluster's surface-brightness distribution or the surface-density distribution is used (see Genzel *et al.* 1994). By varying ρ_0 and the core radius between 0.25 pc and 0.5 pc whilst conserving the total central-parsec mass within errors set by Genzel *et al.* (1996), we find that the collision time-scales for stars (see §3) can vary by up to a factor of 1.5.

We also note that Equation (1) gives quite a flat profile inside the core radius. However, observations become crowded within this radius and it becomes harder to constrain the density distribution. If the condensed mass at Sgr A* is a black hole, theoretical modelling predicts a density cusp at low radii: $\rho \propto r^{-\gamma}$ where $\gamma \sim 1.5 - 2.5$ (Quinlan, Hernquist & Sigurdsson 1995; see also Bahcall & Wolfe 1976). Consequently we also calculate collision rates assuming $\rho \propto r^{-1.8}$ (coinciding with the higher-radius density profile at the GC), which we set equal to the density profile of Genzel *et al.* (1996) for $r \geq 0.38$ pc where we expect the latter to be accurate.

A final comment on Equation (1) is that it is based upon $(M/L)_K = 2$, the mass-to-light ratio evaluated at a few parsecs from the centre. Genzel *et al.* (1996) claim that their usage of only brighter cluster members reduces the effects of population change at lower radii. There does exist some evidence of an increase in $(M/L)_K$ at low radii: Saha *et al.* (1996) show that this ratio may increase by a factor of 3-5 between 2.5 pc and 0.5 pc, although if one subtracts $2.5 \times 10^6 M_\odot$ for the putative central black hole then the increase in $(M/L)_K$ for the cluster only reduces to two.

Collision-rate calculations require a velocity dispersion (see §3). We adopt the deprojected velocity dispersion given by Genzel *et al.* (1996):

$$\sigma^2 = 55^2 + 103^2 (r/10'')^{-1.2} (\text{km/s})^2. \quad (2)$$

The velocity dispersion rises as galactocentric radius falls due to the presence of the supermassive black hole (see also Eckart & Genzel 1997). At higher radii, the enclosed cluster

mass dominates and σ flattens out. Equation (2) is valid throughout the central parsec.

3 COLLISION RATES OF THE CENTRAL-PARSEC STARS

The collision rate per star of species 1 with stars of species 2 is

$$\Gamma_1 = \frac{\Gamma_{12}(r)}{n_1(r)} = n_2(r) \int_0^\infty \Sigma_g(V_\infty, R_{\min}) V_\infty P(V_\infty) dV_\infty \quad (3)$$

where n is the number density of stars and $P(V_\infty)$ is the probability that two stars have *relative* speed V_∞ . Σ_g is the gravitationally focused cross section:

$$\Sigma_g = \pi R_{\min}^2 \left(1 + \frac{2G(M_1 + M_2)}{R_{\min} V_\infty^2} \right) \quad (4)$$

where M_1 and M_2 are the stellar masses and R_{\min} is the collision radius (which we take to be equal to the sum of the radii of the two colliding stars). The second term on the right in Σ_g represents the mutual attraction between two stars which increases the cross section above that of the geometric value. We take $P(V_\infty)$ to be Maxwellian, which is appropriate at high galactocentric radii where the stellar cluster dominates the enclosed mass. In the region where the black hole dominates the enclosed mass (say, $\lesssim 0.7$ pc, see Genzel *et al.* 1996, Eckart & Genzel 1997), $P(V_\infty)$ is still close to Maxwellian (Quinlan *et al.* 1995). At any galactocentric radius we take the *relative* velocity dispersion between two stellar species of any mass to be $2\sigma^2$, where the variation of σ with galactocentric radius is given by Equation (2). In a system of stars that has achieved equipartition of energy, we have $\sigma^2 \propto 1/M$ (see Binney & Tremaine 1987); stars of different masses would have different velocity dispersions. The effects of equipartition on the collision rates do not change our conclusions.

Assuming number-density and velocity-dispersion profiles discussed in §2, Figure 3 shows collision time-scales for the GC. The collision time-scale is a strong function of r and is shortest deep within the core. Comparing Figure 3 with Figure 2 we see that the time-scales for collisions involving giants are similar to the durations for which they are visible at the GC. The collision time-scale for solar-type stars is considerably longer. It is only noticeably less than a Hubble time at very low radii if the density profile is a cusp (*i.e.* within ~ 0.1 pc, assuming $\rho \propto r^{-1.8}$).

The calculations shown in Figure 3 have used an instantaneous radius for the stars. Such calculations lose their meaning, however, if the stellar radius changes on time-scales shorter than the collision time-scale. We now calculate the number of collisions that a star will have by integrating the instantaneous collision rate over its lifetime:

$$n_{\text{coll}} = \int_\tau \Gamma_1 dt. \quad (5)$$

In this way we obtain Table 1 in which we have restricted τ to interesting parts of the star's evolution as well as the entire lifetime, for stars of various masses. We see that n_{coll} , when evaluated over the lifetime of a star, can be a substantial fraction of unity. For sufficiently low radii, and preferably with a steep cusp density profile, n_{coll} is about

Mass [M_{\odot}]	r [pc]	Profile	LIFE	MS	n_{coll}	
					K < 15 ($A_K = 3$)	K < 15 ($A_K = 4$)
1	0.12	G96	0.741	0.292	0.278	0.229
	0.12	cusp	1.74	0.686	0.653	0.538
	0.17	G96	0.549	0.242	0.181	0.148
	0.17	cusp	0.894	0.394	0.295	0.242
1.5	0.12	G96	0.550	0.129	0.320	0.272
	0.12	cusp	1.29	0.302	0.751	0.640
	0.17	G96	0.387	0.106	0.208	0.176
	0.17	cusp	0.631	0.172	0.339	0.286
2	0.12	G96	0.549	0.077	0.340	0.313
	0.12	cusp	1.29	0.182	0.797	0.734
	0.17	G96	0.379	0.0636	0.219	0.201
	0.17	cusp	0.619	0.104	0.358	0.327
4	0.12	G96	0.533	0.0246	0.510	0.508
	0.12	cusp	1.25	0.0576	1.19	1.19
	0.17	G96	0.354	0.0205	0.333	0.333
	0.17	cusp	0.576	0.0335	0.524	0.542
8	0.12	G96	0.909	0.0116	0.900	0.898
	0.12	cusp	2.13	0.0272	2.11	2.11
	0.17	G96	0.589	0.00990	0.582	0.580
	0.17	cusp	0.961	0.0161	0.948	0.945
Durations [yr]						
1			1.25×10^{10}	1.10×10^{10}	5.22×10^7	1.78×10^7
1.5			3.10×10^9	2.73×10^9	4.69×10^7	1.09×10^7
2			1.50×10^9	1.17×10^9	2.73×10^7	4.53×10^6
4			2.15×10^8	1.79×10^8	3.56×10^7	3.52×10^7
8			4.25×10^7	3.72×10^7	9.61×10^6	5.21×10^6

Table 1. Phase durations and number of collisions, n_{coll} , during various evolutionary phases for stars of masses $1 M_{\odot}$, $1.5 M_{\odot}$, $2 M_{\odot}$, $4 M_{\odot}$ and $8 M_{\odot}$ at galactocentric radii of 0.12 pc and 0.17 pc. Profile denotes stellar number-density profile used: G96 refers to the density of Genzel *et al.* (1996) and cusp refers to a density profile of $\rho \propto r^{-1.8}$, set equal to its counterpart at $r \geq 0.38$ pc. We have assumed that the mean mass of the GC stars, \bar{M}_2 , is $1 M_{\odot}$ but note that, approximately, $n_{\text{coll}} \propto 1/\bar{M}_2$. LIFE represents the life-span of the star from ZAMS to AGB termination, MS represents the main-sequence duration and K < 15 represents the time for which the stars are brighter than K=15 for a given extinction. Evolutionary models of stars are from Z=0.02 models from Pols *et al.* (1999).

one. The more-massive stars are more luminous than the $1 M_{\odot}$ star and so spend a larger fraction of their lives as K < 15 magnitude stars. During this period they reach larger radii than $1 M_{\odot}$ stars (Figure 1) and so we expect them to undergo greater proportions of collisions as detectable giants. There are a number of uncertainties in n_{coll} . Uncertainties in the stellar number-density profile are discussed in §2.4. The value of the mean stellar mass (\bar{M}_2) is uncertain. In Table 1 we set the number of impacting stars to be $n_2(r) = \rho_0 n(r)/\bar{M}_2$, where $n(r)$ is given by Equation (1), and where $\bar{M}_2 = 1 M_{\odot}$. Thus, via Equation (3), $\Gamma_1 \propto 1/\bar{M}_2$ (ignoring gravitational focusing). A decrease in \bar{M}_2 to, say, $0.7 M_{\odot}$, increases Γ_1 by a factor ~ 1.4 . n_{coll} is also sensitive to the radius-time behaviour of the stars. Changing the

mass-loss rate by a factor of 10 in the models of Pols *et al.* (1999) produces a factor of two change in n_{coll} .

The relative likelihood of collisions during different phases of the stars' evolution are shown in Figure 4. We see that one of the stars in single-single stellar collisions in the GC will most likely be a giant star (provided that it is sufficiently old to have turned off the main sequence). In terms of collision frequency, the AGB becomes increasingly predominant over the first giant branch for stars of higher mass. Only a minority fraction of target stars are on the main sequence when hit by an impactor. Although the main-sequence phase is much longer lived than the giant phase, more two-body collisions in the GC will occur whilst the target star is a giant because of its much greater radius

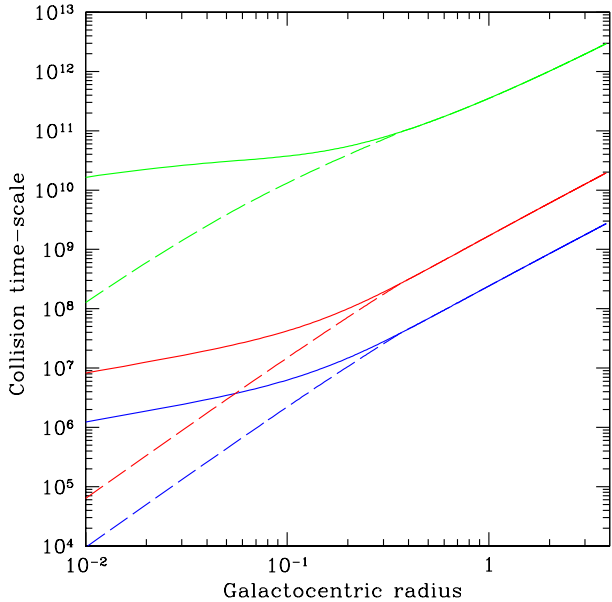


Figure 3. Collision time-scales (in years) for stars in the GC as a function of galactocentric radius (in parsecs). For the calculation we have assumed that the background cluster members are of mass $1 M_{\odot}$, Equation (2) for the velocity dispersion, and for the density profile we have used Equation (1) (solid lines) or $\rho \propto r^{-1.8}$ (dashed lines), set equal to Equation (1) for $r \geq 0.38$ pc. The two lower lines represent the time-scale for encounters for $8 M_{\odot}$ stars at $R_{\min} = 243 R_{\odot}$. The middle two curves represent the time-scale between collisions for $2 M_{\odot}$ stars at $R_{\min} = 94 R_{\odot}$. For comparison, the upper-most lines show the encounter time-scale profile for a $1 M_{\odot}$ star at $R_{\min} = 2 R_{\odot}$.

compared to the main-sequence radius. In fact the number of target stars on the main sequence is $\lesssim 25\%$, with the exception of 45% for a $1 M_{\odot}$ star. The importance of the main-sequence phase decreases with increasing stellar mass. The horizontal branch also generally dominates over the main sequence in competition for collisions: it is shorter-lived but the star is considerably larger on the horizontal branch than when on the main sequence.

4 CRITERIA FOR DESTRUCTION OF GIANTS

To determine whether stellar collisions may destroy giant stars, one needs to know how much envelope mass a giant must lose before it is destroyed. Strictly speaking, to satisfy the observed paucity we must strongly reduce the K-magnitude of the brightest giants. Considering mild encounters where the mass lost is insufficient to alter the giant's long-term evolution, we actually expect a transient *increase* in the stellar K-luminosity: the impactor loses some of its kinetic energy to the envelope which consequently expands somewhat, becomes redder and therefore brighter in the K-band. The envelope will then settle back to normal on its thermal time-scale (\sim few-hundred years). To explain the paucity of giants, collisions must therefore destroy the giant, *i.e.* they must cause large amounts of envelope loss. The actual amount of mass loss required as a direct result

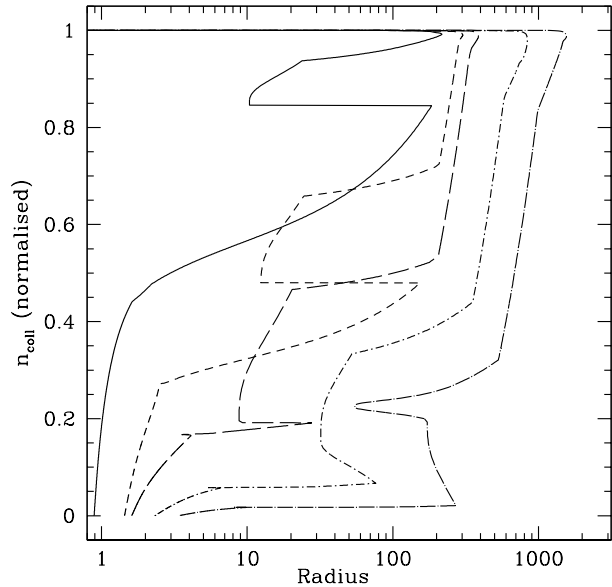


Figure 4. The distribution of collisions, n_{coll} (normalised), during the lifetimes of stars of various masses, plotted as a function of the stellar radius (solar units), which emphasises different evolutionary stages. The solid line represents a $1 M_{\odot}$ star, the short-dashed curve represents a $1.5 M_{\odot}$ star, the long-dashed curve corresponds to a $2 M_{\odot}$ star, the short-dashed, dotted line represents a $4 M_{\odot}$ star and the long-dashed, dotted curve corresponds to an $8 M_{\odot}$ star. We have assumed that all impinging stars are solar mass and solar radius, and have adopted $\sigma = 183.13$ km/s, appropriate for a galactocentric radius of 0.17 pc.

of a collision is uncertain but is likely to be most if not nearly all of the envelope (Eggleton, Tout, private communications). A second way to destroy the giant is via indirect mass loss after a collision produces a common envelope system. In such systems, the binding energy released by the impactor and core spiralling in towards each other may unbind the envelope. To form a common envelope system in a hyperbolic collision requires the impactor to deposit at least $\mu V_{\infty}^2/2$ of its orbital energy into the giant but need not necessarily produce copious mass loss. Thus to destroy a giant, a collision must involve either immediate, large mass losses or the formation of a common envelope system which then evolves to expel the envelope (§7).

5 APPROACH TO HYDRODYNAMICAL SIMULATIONS

We simulated encounters involving giant stars using a smoothed-particle hydrodynamics (SPH) code. For a discussion of SPH, see Benz (1990). The impactors encountering the star were point masses which were adequate to simulate either main-sequence stars or compact remnants such as white dwarfs, neutron stars or stellar black holes because of the size contrast between these objects and the giant's envelope.

5.1 Collisions performed

We performed collisions on two red giants. The radii and luminosity of the stars were selected so that their positions on a HR diagram coincided with those of the missing bright giants (see Figure 1). One giant had mass $2 M_{\odot}$, radius $94 R_{\odot}$ and core mass $0.52 M_{\odot}$. The other giant had mass $8 M_{\odot}$, radius $243 R_{\odot}$ and core mass $2.5 M_{\odot}$. In each case we represented the core by a point mass. The masses of the two stars were selected so that we sampled both ends of the likely mass range of the missing giants (see §2). Both giants were based upon models of temperature and density profiles discussed in Pols *et al.* (1995).

Most simulations were performed with ~ 8500 particles. A number of simulations were run with 16×10^3 and 36×10^3 particles in order to quantify resolution effects (see §6.3). A wide range of impactor masses were selected. For the $2 M_{\odot}$ giant we used $0.6 M_{\odot}$, $1 M_{\odot}$, $1.4 M_{\odot}$, $2 M_{\odot}$, $4 M_{\odot}$ and $8 M_{\odot}$ impactor masses. Our results suggested that for the $8 M_{\odot}$ giant, results from impacts with a $1 M_{\odot}$ impactor would be quantitatively similar to the outcomes of the giant's encounters with $0.6 M_{\odot}$ and $1.4 M_{\odot}$ impactors, so for the more-massive giant we simulated collisions involving only $1 M_{\odot}$, $2 M_{\odot}$, $4 M_{\odot}$ and $8 M_{\odot}$ impactors.

For each giant-impactor pair, we ran $\sim 16 - 25$ simulations distributed on a $V_{\infty} - R_{\min}$ grid. A number of simulations were also performed very near the V_{∞} and R_{\min} axes in order to quantify our extrapolations from the grid to low V_{∞} and low R_{\min} values (see §6.3). In total approximately 200 runs were performed.

5.2 Quantifying collision outcomes

To determine whether a collision destroyed the giant, we measured the mass loss, ΔM , searching for mass losses of most of the envelope (§4). To determine ΔM , the enthalpy of each particle was evaluated relative to both the impactor and the giant, using a similar method as prescribed in Rasio & Shapiro (1991). For each collision we ascertained the amount of mass remaining bound to the giant, the amount that had become bound to the impactor and the amount of escaping matter. We found that ΔM settled down within a sound-crossing time or two after a collision.

A number of collisions involved dissipation of enough of the impactor's orbital energy for the impactor to become bound to the giant. Such systems are important as they potentially lead to the destruction of the giant via a common envelope phase (§6.2). To delimit the region of the $V_{\infty} - R_{\min}$ plane in which two impactors became bound, we measure the fractional change in their orbital energy, $\Delta E/E$. We define ΔE such that $\Delta E/E = 1$ when the impactor just becomes bound to the giant. The initial orbital energy is simply $\mu V_{\infty}^2/2$; the final orbital energy is calculated from the masses, positions and velocities of the two centres of mass.

For some of the bound systems formed, the impactor remained inside the envelope, *i.e.* a common envelope system had effectively been formed immediately. In such systems we do not have two distinct objects to which we can assign fluid particles. Our algorithm is thus unsuitable for such outcomes and so ΔM and $\Delta E/E$ were not measured for these outcomes.

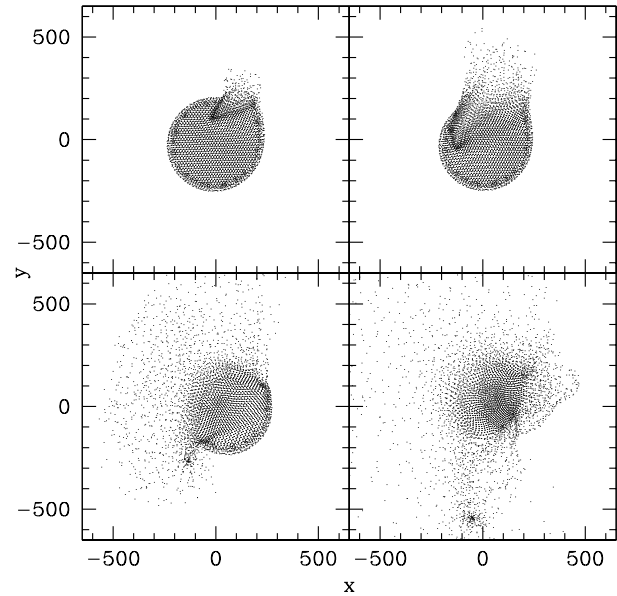


Figure 5. Time sequence of fluid-particle plots of an SPH simulation between an $8 M_{\odot}$ giant and a $1 M_{\odot}$ impactor (centre-of-mass frame), with $V_{\infty} = 50$ km/s and $R_{\min} = 100 R_{\odot}$. Here we take a slice in the plane of the collision. The trajectory of the impactor is clearly deflected; this is due to the giant's mass enclosed in its orbit. The top-left and top-right portions in particular show the shock caused by the impact. Units of x and y are solar radii.

6 RESULTS

The impactor hits the giant supersonically, shocking the envelope, as can be seen in Figure 5. Due to the giant's gravity, the impactor is pulled around the core somewhat; the amount of deflection depending on the V_{∞} of the encounter. Almost all of the escaping particles had speeds in excess of the local escape speed ($V_{\text{esc}} = \sqrt{2GM_1/R}$ for $R \geq R_1$, where R_1 is the giant's radius), demonstrating that the escaping fluid was energetically unbound by virtue of its kinetic energy rather than its thermal energy. Some fluid had speeds up to four times that required to escape and thus carried off excess energy thereby reducing the mass loss. Given that mass losses are generally low (§6.1), this implies that deep collisions are required to remove envelope material located close to the core.

Both mass loss from the giant and orbital energy loss from the two stars increase with increasing impactor mass and with decreasing V_{∞} , indicating the dominance of time-dependent gravity over shocks as the energy-transfer mechanism. Mass loss and orbital energy loss also increase with decreasing R_{\min} .

We divide the collision outcomes into two categories: bound and unbound giant-impactor pairs (after collision). A bound system is defined by $\Delta E/E \geq 1$ (see §5.2). Both mass loss (Figure 6) and orbital energy loss seemed to vary smoothly across the boundary (Figure 7).

6.1 Mass loss

We reiterate that the instantaneous mass loss increases with impactor mass and falls with increasing V_{∞} and R_{\min} . For

two given colliding species, this implies that we would observe maximal mass loss for collisions of lowest V_∞ and lowest R_{\min} . Those particular encounters, however, tended to directly produce common envelope systems (see §6.2) for which we do not measure the mass loss due to the collision. Consequently the subsequent comments concerning ΔM are limited to outcomes that are not common envelope systems and that constitute the larger portion of our data.

Collisions of both giants with impactors of mass $\sim 1 M_\odot$ involved small mass losses, $\lesssim 0.1 M_\odot$ (and usually much less, see Figure 6). In fact, for the $8 M_\odot$ giant and for $V_\infty \gtrsim 100$ km/s, the mass losses were so small that too few SPH particles escaped to take a reliable measurement of ΔM . Even deep impacts ($R_{\min} \sim R_1/4$) were not devastating for either giant, although the mass lost from the $2 M_\odot$ giant rose to $\sim 0.1 M_\odot$.

If the bulk of the population in the GC are stars of masses $\lesssim 1 M_\odot$, then the paucity of bright giants cannot be explained by instantaneous mass loss due to two-body collisions because the vast majority of collisions with $1 M_\odot$ impactors will involve mass losses much less than the envelope mass.

Mass losses were higher for more-massive impactors because of the greater gravitational forces involved. We discuss here the effects of $8 M_\odot$ impactors. Encounters involving our $8 M_\odot$ giant showed mass losses of $\sim 0.1 - 1 M_\odot$ for $R_{\min} \gtrsim 50 R_\odot$. Collisions involving the $2 M_\odot$ giant with $R_{\min} > 25 R_\odot$ gave mass losses $\lesssim 0.5 M_\odot$, dropping to a few $\times 10^{-2} M_\odot$ for fast ($250 - 450$ km/s) grazing encounters. Deeper impacts had much stronger effects for both giants. For our $8 M_\odot$ giant, collisions with $R_{\min} < 50 R_\odot$ gave rise to mass losses of about $3 M_\odot$ for $V_\infty \gtrsim 150$ km/s (our slower collisions gave rise to common envelope systems). For the $2 M_\odot$ giant, encounters of $R_{\min} \lesssim 25 R_\odot$ involved mass losses approaching the entire envelope mass. It is possible that low R_{\min} ($\lesssim 30 R_\odot$) collisions with massive impactors could destroy the giants. Such collisions, however, will be rare; considering the low R_{\min} alone places *upper limits* of frequencies of 5% of all giant- $8 M_\odot$ impactor collisions for the $8 M_\odot$ giant and 20% for the $2 M_\odot$ giant, assuming that all collisions occur at $V_\infty = \sqrt{2}\sigma(r)$ and that $r = 0.2$ pc. We note that in §3 we showed that a star could expect at most about one collision before becoming a remnant; most collisions will occur at too high R_{\min} to destroy the giant. Moreover, to destroy all giants in this manner would further require the GC to contain a large proportion of impactors of masses $\gtrsim 8 M_\odot$. Such a population seems quite unlikely, unless, perhaps, the GC core is dominated by massive black holes which have diffused inwards from higher galactocentric radii (see §2 and Morris 1993).

In summary, mass losses due to most two-body collisions are likely to be small ($\lesssim 0.1 M_\odot$), and though very massive impactors might be able to destroy the giants, the deep-envelope collisions required will make such encounters rare, unless the GC contains an exotic population of numerous massive stars which is itself unlikely.

6.2 Formation of bound systems

For collisions of sufficiently low V_∞ and R_{\min} , the impactor lost enough kinetic energy to become bound to the giant. Such collisions will almost always be physical collisions and

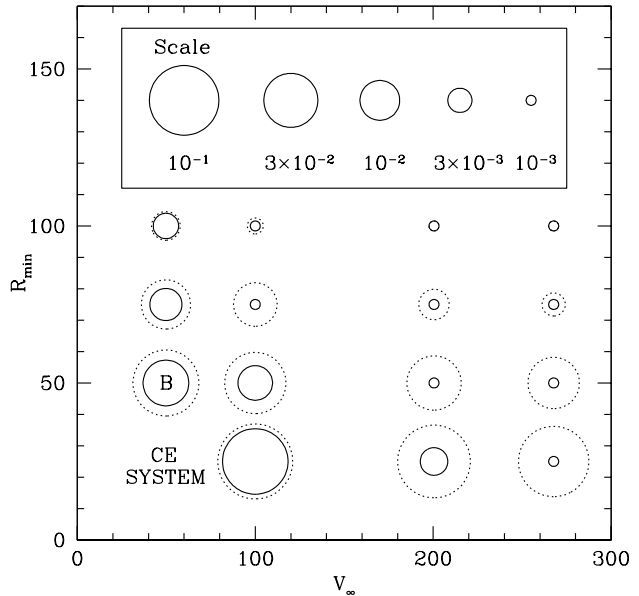


Figure 6. Impactor-accreted mass (unbroken circles) and mass lost from the system in collisions (broken circles) between the $2 M_\odot$ giant and a $1 M_\odot$ impactor, as a function of V_∞ [km/s] and R_{\min} [R_\odot]. The symbol “B” represents that the collision product is a binary, and “CE SYSTEM” denotes the direct formation of a common envelope system. The size of the circles is proportional to the log of the mass. Masses are in solar units.

we expect the resulting orbits’ periastrons to remain inside the giant. If the apastron of the orbits were also within the giant’s radius then a common envelope system had effectively immediately been formed. Systems with apastrons outside the giant’s envelope were very eccentric and had periods of a few years to centuries. Thus the time-scale for further collisions is much shorter than the giant’s evolution time-scale. We expect each subsequent encounter to dissipate more of the orbital energy until the apastron falls within the giant’s radius (or the envelope puffs up enough to absorb the impactor’s orbit), producing a common envelope system.

Common envelope systems are of great interest here as their evolution may quickly destroy the giant. The impactor and giant’s core spiral towards each other, transferring angular momentum and energy to the envelope. If a sufficient quantity of the potential energy between the impactor and giant’s core is deposited into the envelope, the entire envelope may be expelled, leaving a tight binary. Alternatively, the impactor may merge with the core before envelope ejection is complete, terminating the common envelope phase. The outcomes of common envelope evolution involving either of the two giants considered here are discussed in §7, here we calculate the fraction of collisions that produce them.

Figure 7 shows the dependence of the fractional change in pre-collision orbital energy on V_∞ and R_{\min} for a certain giant-impactor pair. Bound systems are produced in the bottom-left of the Figure and are delimited from unbound systems by the $\Delta E/E = 1$ contour (which we now denote as $R_b(V_\infty)$). As impactor mass increases, the de-

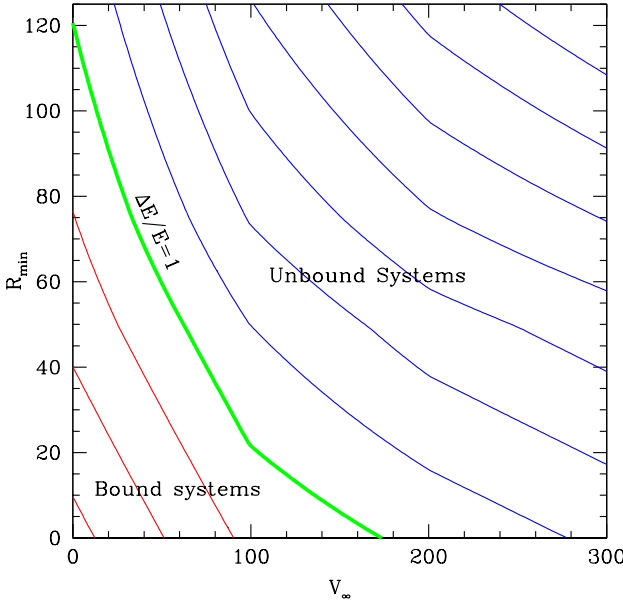


Figure 7. $\Delta E/E$ contour plot for collisions involving the $2 M_\odot$ giant and a $1 M_\odot$ impactor, as a function of V_∞ [km/s] and R_{\min} [R_\odot]. The contours are logarithmically spaced by 0.5, the bold line represents $\Delta E/E = 1$ i.e. the threshold of bound-system formation. Contours to the bottom-left of this line have $\Delta E/E > 1$ so the bottom-left region represents the region where bound systems are formed. Collisions of the upper-right portion leave the two stars unbound.

limiting contour moves toward the top-right portion of the Figure. Values of $\Delta E/E$ between data points are obtained by linear interpolation of a fitted 2D exponential function $\Delta E/E(V_\infty, R_{\min})$. Note we do not measure $\Delta E/E$ for common envelope systems, rather, we extrapolate from the other data. The fraction of collisions, f_{ce} , that fall underneath the $R_b(V_\infty)$ curve depends on the likelihood of having a given velocity (V_∞) and therefore on $P(V_\infty)$, the velocity distribution function, which we take to be Maxwellian (§3). For a given V_∞ , f_{ce} depends on the proportion of collisions that have $R_{\min} \leq R_b(V_\infty)$ and thus depends on the amount of gravitational focusing (Equation [4]):

$$f_{\text{ce}} = \frac{\int_0^\infty \Sigma_g(V_\infty, R_{\min} = R_b(V_\infty)) V_\infty P(V_\infty) dV_\infty}{\int_0^\infty \Sigma_g(V_\infty, R_{\min} = R_1) V_\infty P(V_\infty) dV_\infty}. \quad (6)$$

The dependence of $\sigma(r)$ on position within the GC exerts a galactocentric radial dependence on f_{ce} and is shown in Figure 8.

We see that f_{ce} increases with impactor mass, which follows because the increased gravitational interaction allows bound systems to be formed at both higher speeds and at higher R_{\min} . Figure 7 shows that for increasing V_∞ , the largest R_{\min} that produces a bound system decreases. As galactocentric radius decreases, the median V_∞ increases and so we expect f_{ce} to decrease rapidly inside the core radius (~ 0.38 pc) and to flatten at high radii in accordance with the nature of the velocity dispersion (Equation [2]), as illustrated by Figure 8. Within the core radius the fraction of bound systems formed is only a few percent ($\sim 1 - 10\%$ at the core radius). At a few parsecs, $f_{\text{ce}} \sim 10 - 40\%$ for

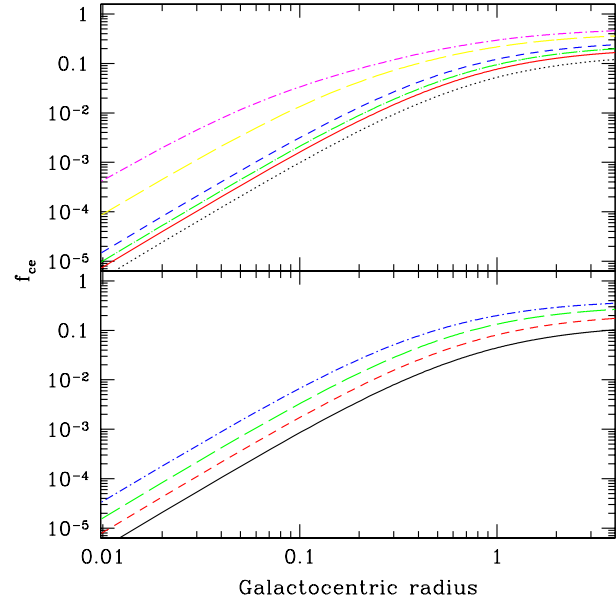


Figure 8. The fraction of encounters that produce bound systems as a function of galactocentric radius (in parsecs): the $8 M_\odot$ giant (lower half) and the $2 M_\odot$ giant (upper half). Different curves reflect different impactor masses with curves of increasing height representing increasing impactor mass. For the $8 M_\odot$ giant, the impactor masses are $1 M_\odot$, $2 M_\odot$, $4 M_\odot$ and $8 M_\odot$. The same notation has been used for the $2 M_\odot$ giant, except we also show curves for $0.6 M_\odot$ impactors (dotted line) and $1.4 M_\odot$ impactors (dot-dashed line). We have used Equation (2) to describe $\sigma(r)$.

the range of impactor masses considered. The large f_{ce} at high galactocentric radii is due to the low local velocity dispersion.

We note that f_{ce} is substantially less than one, even for collisions between the $8 M_\odot$ giant with $8 M_\odot$ impactors at high galactocentric radii (i.e. low speeds). Since f_{ce} is the fraction of physical collisions that lead to the capture of the impactor, for tidal capture to occur we require $f_{\text{ce}} > 1$. Thus tidal capture by giants similar to those discussed here will be extremely rare in the galactic centre.

6.3 Resolution and error considerations

Three sources of error in our data were considered: the accuracy of extrapolation of $\Delta E/E$ to regions near the V_∞ and R_{\min} axes (Figure 7), errors in energy conservation in individual SPH runs and errors due to resolution effects (i.e. number of particles used) in our simulations.

To assess errors in $\Delta E/E$ extrapolation we performed a number of simulations near the V_∞ and R_{\min} axes and compared the local extrapolated $\Delta E/E$ value to that obtained from the extra runs. We then locally refitted $R_1(V_\infty)$ and re-calculated f_{ce} to evaluate its error. Errors in f_{ce} due to energy conservation in individual runs were examined by estimating their effects on the local $\Delta E/E$ value and hence on the locus of the $R_b(V_\infty)$ contour, producing an error in f_{ce} . In both cases the error in f_{ce} for all giant-impactor pairs throughout most of the GC is within $\pm 30\%$. Slightly over-widely spaced grids for the $2 M_\odot$ giant and $2 M_\odot$, $4 M_\odot$ and

$8 M_{\odot}$ impactors led to larger errors at low galactocentric radii, but the net effect is likely to be a mild overestimation (within a factor of two) of f_{ce} for any galactocentric radius outside of the central few hundredths of a parsec. These errors do not weaken our conclusions; indeed, overestimation of f_{ce} actually acts to strengthen our conclusions (see §8).

We also estimated errors in ΔM and $\Delta E/E$ (and hence f_{ce}) due to resolution, *i.e.* using a limited number of particles in our simulations. We repeated a quantity of collisions involving the $8 M_{\odot}$ giant with 16×10^3 and 36×10^3 particles. The quantity of interest (*e.g.* ΔM) was evaluated as a function of the particle separation. Extrapolation to zero spacing (*i.e.* infinite resolution) obtains the best estimate of the quantity. We found that our mass losses became generally good estimates for $\Delta M \gtrsim \text{few} \times 0.01 - 0.1 M_{\odot}$, depending on impactor mass. The resolution errors in $\Delta E/E$ caused uncertainties in f_{ce} that were generally small and never large enough to affect our conclusions. Since the $2 M_{\odot}$ giant shows, to some extent, similar scaling to the $8 M_{\odot}$ giant (*e.g.* number of particles per fractional radius), we expect similar resolution errors.

The uncertainties considered here do not affect our conclusions, and so we have not included them in our calculations.

7 EVOLUTION OF BINARY SYSTEMS FORMED

We now consider the outcomes of the evolution of common envelope systems formed by our two-body encounters. Within the envelope, the core and impactor orbit each other in ever tightening orbits, their potential energy being converted into their orbital kinetic energy and thence deposited in the envelope. If the envelope gains enough energy, it will become unbound. We take the binding energy of the envelope to be (de Kool 1990):

$$E_{\text{env}} = \frac{G(M_c + M_{\text{env}})M_{\text{env}}}{\lambda R_{\text{env}}} \quad (7)$$

where M_c is the giant's core mass, M_{env} and R_{env} are respectively the envelope's mass and radius and we take λ to be 0.5. The change in binding energy between the impactor and the giant from the onset of common envelope evolution to its termination when the entire envelope has been expelled is given by:

$$\Delta E_{\text{fi}} = \frac{GM_2M_c}{2d_i} - \frac{GM_2(M_c + M_{\text{env}})}{2d_f} \quad (8)$$

where M_2 is the impactor mass, d_i and d_f are the initial and final semi-major axes. By assuming all the envelope is removed with some efficiency, α , then

$$E_{\text{env}} = \alpha \Delta E_{\text{fi}}. \quad (9)$$

Thus we may calculate the final separation between the impactor and core:

$$d_f = M_c \left(\frac{2E_{\text{env}}}{G\alpha M_2} + \frac{M_c + M_{\text{env}}}{d_i} \right)^{-1}. \quad (10)$$

The following results are insensitive to d_i since d_i must be very deep in the envelope before the second right-hand term becomes comparable to the first. Numerical modelling of common envelope evolution suggests that $\alpha \sim 0.24 - 0.6$

(Taam & Bodenheimer 1989, Sandquist *et al.* 1998); we take $\alpha = 0.4$. Using the parameters for our giants (see §5), for both giants we find that d_f takes values between $\sim 0.8 - 4 R_{\odot}$ for impactor masses in the range $0.6 M_{\odot}$ to $3 M_{\odot}$. d_f is similar for both giants because the greater energy required to unbind the $8 M_{\odot}$ giant's envelope is offset by the greater energy released by an impactor falling towards its more massive core.

We have thus far assumed that the core and impactor are point masses. Their sizes, however, can be important and can lead to termination of the common envelope phase before total ejection of the envelope. Either the impactor or the core may fill their Roche lobes or, alternatively, the impactor may fall so deep into the giant that the local density is comparable to its own. In the following calculations we find the former almost always occurs before the latter. Either way, the impactor is no longer distinct from its surroundings and no further potential energy may be liberated. The occurrence of such "premature" termination depends on the size of the impactor and the other parameters in Equations 7-10. We ascertain whether envelope ejection will occur in the following way. Two species of impactor are considered: ZAMS stars and stellar remnants. The radii of the former are taken from Tout *et al.* (1996). A simple mass-radius relation for white dwarfs suffices for this discussion: $R \propto M_1^{-1/3}$ ($M_1 < 1.4 M_{\odot}$), scaled to $0.0248 R_{\odot}$ at $1 M_{\odot}$. More-massive remnants (neutron stars) are given a size of 10km. We calculate the impactor's Roche-lobe size using Eggleton (1983):

$$\frac{R_{\text{L1}}}{d_f} = \frac{0.49q^{\frac{2}{3}}}{0.6q^{\frac{2}{3}} + \ln(1 + q^{\frac{1}{3}})} \quad (11)$$

where $q = M_2/M_c$. Finally, we used the density profiles of our giant models (see §5) to determine the giant's radius at which the density was comparable to that of the impactor's density (derived from its mass and the appropriate mass-radius relation). Our results are shown in Figure 9.

We see that for $\alpha \sim 0.5$, ZAMS stars of masses $\gtrsim 1 M_{\odot}$ may expel the envelope of the $2 M_{\odot}$ giant, whereas ZAMS stellar masses in excess of $2 M_{\odot}$ are required to expel the $8 M_{\odot}$ giant's envelope. Increasing α decreases the minimum mass required. We also see that a ZAMS star will always fill its Roche lobe before penetrating sufficiently deep into the envelope for the local density to be comparable to its own. Stellar remnants should almost always be able to eject the envelopes of either star, the exception being for low-mass ($\lesssim 0.4 M_{\odot}$) remnants with the $8 M_{\odot}$ giant. If α is very low, the core will generally fill its Roche lobe before a remnant counterpart does, except in the case of the $2 M_{\odot}$ giant with remnants of masses $\lesssim 0.5 M_{\odot}$. This is because the $2 M_{\odot}$ giant's core (of mass $0.52 M_{\odot}$) is essentially a white dwarf and white dwarfs of lower masses are larger: they will fill their Roche lobes first. A similar effect is not seen for the $8 M_{\odot}$ giant: its core is much larger ($0.25 R_{\odot}$) than a stellar remnant and tends to fill its Roche lobe first.

It seems likely that most *low-mass* main-sequence stars will not expel either of the giants' envelopes, particularly that of the $8 M_{\odot}$ giant. The numbers of common envelope systems formed by two-body encounters that lead to total envelope expulsion will therefore be dependent on the remnant fraction in the GC population (see §2). To be sure that most common envelope systems will expel the envelope

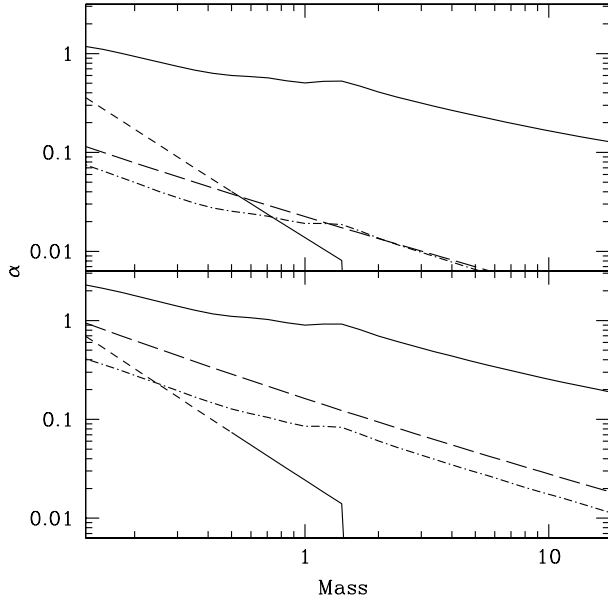


Figure 9. Envelope-ejection efficiency, as a function of impactor mass [M_{\odot}], for which the envelopes of our giants may be expelled before the impactor sinks deep enough into the giant that the impactor or the core fills its Roche lobe or the density of the giant becomes comparable to that of the impactor. The lower box represents the $8 M_{\odot}$ giant and the upper box represents the $2 M_{\odot}$ giant. For each giant, the upper-most (solid) line corresponds to Roche-lobe filling by ZAMS impactors. The lower, solid line represents Roche-lobe filling by stellar remnants; the broken region represents remnants that, if they exist, must be produced in a binary since their solitary progenitors live longer than a Hubble time. The almost vertical drop in the remnant curve corresponds to the Chandrasekhar mass limit ($\sim 1.44 M_{\odot}$), above which the remnants are neutron stars (or black holes for even larger remnant masses) and, effectively, are point masses requiring very low α to eject the envelope. The long-dashed line represents Roche-lobe filling of the giant's core and the dot-dashed line represents the efficiency at which the ZAMS star falls deep enough into the envelope that the local density matches its own.

lope requires a population with a large abundance of stellar remnants or massive main-sequence stars with few low-mass main-sequence stars; such a population may exist in the GC if the star-formation low-mass cut-off is high (*e.g.* $> 0.8 M_{\odot}$) or if the GC contains an extra population of neutron stars and black holes (Morris 1993).

The violence of this method of forming common envelope systems may partly assist in lowering the impactor-mass limit for full envelope expulsion. Although the energy deposited in the envelope to make the impactor bound ($\mu V_{\infty}^2/2$) will dissipate on the envelope's thermal time-scale of a few-hundred years (perhaps somewhat shorter than common envelope evolution), the mass loss, however, is permanent. Both effects tend to lower the envelope's binding energy. In both cases, though, the effects are strongest for massive impactors (which are likely to eject the envelope anyway) and are weakest for low-mass impactors.

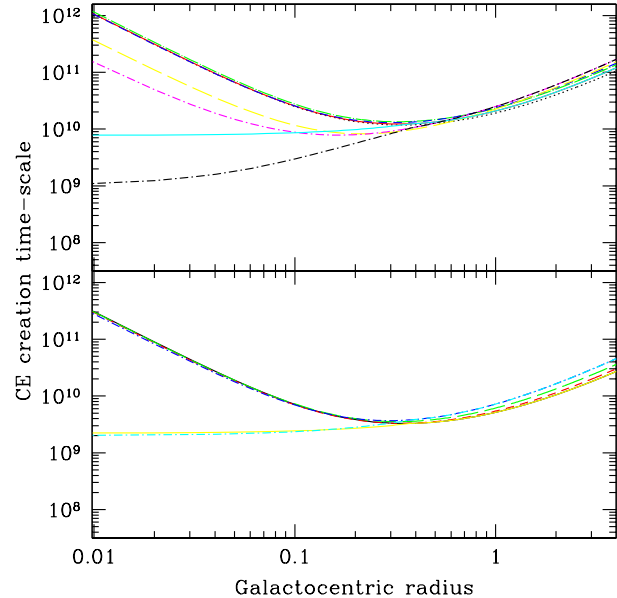


Figure 10. Time-scales [years] for the creation of bound systems in the galactic centre. The lower graph represents time-scales for the $8 M_{\odot}$ giant and the upper graph corresponds to the $2 M_{\odot}$ giant. In each case, the solid line represents $1 M_{\odot}$ impactors, the short-dashed line shows time-scales for $2 M_{\odot}$ impactors (this curve is partly concealed by the solid line for the upper figure), the long-dashed line denotes the $4 M_{\odot}$ impactors and the dot-dashed line corresponds to $8 M_{\odot}$ impactors. In addition, in the $2 M_{\odot}$ giant portion the dotted curve represents collisions with $0.6 M_{\odot}$ impactors and the long-dashed dotted curve shows the bound-system creation time-scales with $1.4 M_{\odot}$ impactors. We have used the velocity dispersion and density profile of Genzel *et al.* (1996). For both target giants, the two less-bold sets of curves (which point to low time-scales at low galactocentric radii) correspond to impactor masses of $1 M_{\odot}$ (solid line) and $8 M_{\odot}$ (dot-dashed line), but we have replaced the density of Genzel *et al.* (1996) by the $\rho \propto r^{-1.8}$ profile (see §2.4).

8 DISCUSSION: TIME-SCALES FOR FORMING COMMON ENVELOPE SYSTEMS

The time-scale for a giant to undergo a two-body collision that forms a bound system is given by

$$\tau_{ce}(r) = \frac{1}{\Gamma_1(r)f_{ce}(r)} \quad (12)$$

where $f_{ce}(r)$ is the fraction of collisions that form bound systems and $\Gamma_1(r)$ is the collision rate per giant, given by Equation (3). If all such bound giant-impactor pairs develop into common envelope systems (see §6) which then evolve to expel the envelope, τ_{ce} is then a lower limit for the destruction of our giants in the GC, excluding the rare collisions in which the instantaneous mass loss approached the total envelope mass (§6). We minimise τ_{ce} by assuming that, for a given impactor mass, M_2 , *all* stars in the GC (other than our giant) are of mass M_2 . This produces Figure 10 where we see that for both giants $\tau_{ce} > 10^9$ years, even if $n \propto r^{-1.8}$. This time-scale is longer than the lifetimes of stars of masses $\gtrsim 2 M_{\odot}$. Given the rarity of high mass-loss encounters, we conclude that the paucity of luminous red-giant stars is un-

likely to be due to two-body encounters involving AGB stars of mass $\sim 2 - 8 M_{\odot}$, whether via dramatic, instantaneous mass loss or via forming a common envelope system (after a collision) which then evolves to expel the envelope. This conclusion does not exclude the possibility of collisions involving pre-giant stars. We also note that collisions involving binaries may be another way to destroy giant or pre-giant stars (see §9 and Davies *et al.* 1998).

The broad minima in Figure 10 are due to competition between $\Gamma_1(r)$ and $f_{ce}(r)$. The former is high at low galactocentric radii and decreases outwards, following the trends of the velocity dispersion and density profile. $f_{ce}(r)$ is highest when the velocity dispersion is lowest (§6.2). The outcome is a minimum at about $r = 0.3$ pc, coincidentally just outside the region of the observed paucity.

Another feature is the narrow spread in τ_{ce} with impactor mass. Note that the curves for the $2 M_{\odot}$ giant encountering $2 M_{\odot}$, $4 M_{\odot}$ and $8 M_{\odot}$ impactors may be underestimating τ_{ce} somewhat [§6.3]. If τ_{ce} is independent of M_2 , then $f_{ce} \propto M_2$ because $\tau_{ce} \propto 1/(\Gamma_1 f_{ce}) \propto M_2/(\rho f_{ce})$. Including corrections for uncertainties in $f_{ce}(r)$ (see §6.3) shows that τ_{ce} varies by less than a factor of 2.5 with M_2 across a wide range of radii. Clearly τ_{ce} is only weakly dependent on M_2 .

9 FURTHER EXPLANATIONS FOR THE OBSERVED DEPLETION OF GIANTS

9.1 Eccentric orbits

In the calculations of time-scales for two-body collisions involving giant stars we have assumed that the stars are on circular orbits, *i.e.* constant galactocentric radii, and so, for a given star, the collision rate is uniform in time. A thermalised stellar system, however, has a distribution of eccentricities, and so a number of giant stars will be on orbits that take them very deep into the GC. If the stellar number-density profile is cusp-like (see §2.4) then the collision rate in the deep core will be very high, suggesting that giants on such orbits could be destroyed via collisions when near their perigees. The time spent by the giants near the perigee is, however, short, and preliminary investigation suggests that unless the cusp-like density profile ($\rho \propto r^{-1.8}$) assumed here significantly underestimates the actual density profile, then the number of devastating collisions involving giants will be insufficient to account for the observed paucity, even if the impactors are massive black holes rather than solar-mass stars.

Main-sequence stars as well as giants can be on eccentric orbits that take them deep into the GC, and so possibly the progenitors of the giants may be destroyed in collisions. Figure 3 suggests that collisions involving main-sequence stars could become frequent in the deep GC if the number-density of stars is cusp-like. Considering main-sequence stars on eccentric orbits of semi-major axes of about 0.12 pc, the numbers of collisions that they will undergo in the deep GC is too small to account for the total absence of bright giants as observed by Genzel *et al.* (1996). It is worth noting, however, that the longevity of low-mass main-sequence stars indigenous to very low galactocentric radii allows them to undergo several collisions.

9.2 Mass segregation

Stars of mass greater than the local mean mass will tend to sink deeper into the potential well via dynamical friction: mass segregation will occur. Mass-segregation occurs on a time-scale similar to the relaxation time, which for a star of given mass M , is given by:

$$\tau_{rel} = \frac{0.34\sigma(r)^3}{G^2 M \rho(r) \ln \Lambda} \quad (13)$$

(see Binney & Tremaine 1987), and thus depends on the local values of density, velocity dispersion and Λ , the Coulomb potential. As τ_{rel} may be a function of radius in the GC, so also will be the mass-segregation rate, which may be estimated as (Hut *et al.* 1992):

$$\frac{dr}{dt} \sim -\frac{r}{\tau_{rel}(r)}. \quad (14)$$

Thus the time taken for a star's orbit to segregate from radius r_i to r_f is

$$\tau_{seg} = -\frac{0.34}{G^2 M} \int_{r_i}^{r_f} \frac{\sigma^3 dr}{r \rho \ln \Lambda}. \quad (15)$$

For mass segregation to be of interest to the collisional destruction of stars, we require $\tau_{seg} \leq \tau_m$, where τ_m is the lifetime of a star of mass M . If a given star sinks significantly during its lifetime, then the increase in collisions that it will undergo in high-density regions could become important. Disregarding the contribution from Λ , $\tau_{seg} \propto 1/M$; stars of higher mass sink more quickly than those of lower mass. However, τ_m decreases strongly with M , so that for $8 M_{\odot}$ stars sinking from radii of 0.1–0.2 pc, the increase in the numbers of collisions is too small to account for the absence of the bright giants (Genzel *et al.* 1996), if such giants were $8 M_{\odot}$ stars. Stars of lower masses, say $2 M_{\odot}$ and $4 M_{\odot}$, live sufficiently long for significant mass segregation to occur, as Figure 11 shows. The cusp-like density profile gives shorter segregation times than the profile of Genzel *et al.* (1996) because the slope of the former tends to offset the increasing Keplerian ($\sigma \propto r^{-0.5}$) velocity dispersion as radius decreases, whereas the latter profile is essentially flat at low radius and so the increasing velocity dispersion actually gives rise to lower sinking rates as radius decreases.

Although the flatter density profile of Genzel *et al.* (1996) may allow $2 M_{\odot}$ and $4 M_{\odot}$ stars to sink some distance during their lifetimes, the collision rates do not increase strongly enough to make a difference compared to the case of a star that remains at a constant galactocentric radius of about 0.12 pc; this is a consequence of the profile's flatness (Figure 3). The cusp-like profile, however, not only allows stars to sink more deeply into the GC but also provides a strongly increasing collision rate. Assuming the cusp-like profile, during its lifetime a $4 M_{\odot}$ star may sink down to about 0.02 pc if it were created at 0.12 pc. By virtue of their longevity, stars of mass $2 M_{\odot}$ may sink to within 0.01 pc in the cusp-like profile, even if they were born at 0.17 pc. Whilst mass segregating inwards, both stars will undergo the majority of collisions whilst on the giant branch, *i.e.* during the latter stages of their lives after they had had time to sink some distance. A giant star that has mass segregated from a certain galactocentric radius will have more collisions than an unsegregated giant star on an eccentric orbit because the former will spend all its life at low galactocentric radii

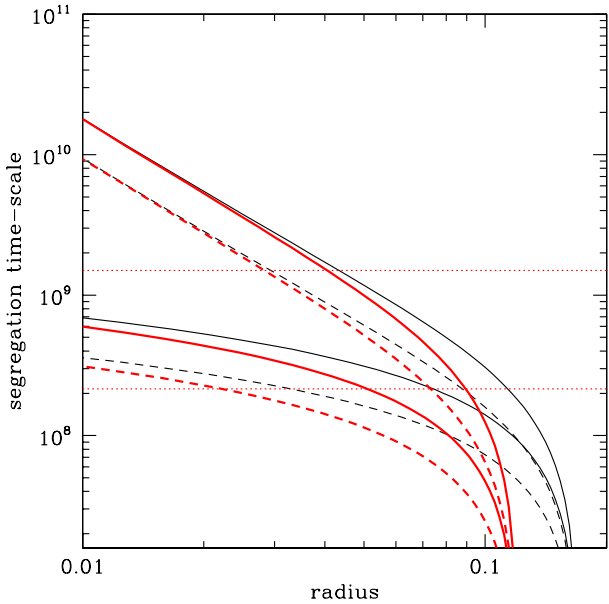


Figure 11. Mass segregation time-scales [in years] for stars as a function of galactocentric radius [parsecs]. The time measured is the time taken to sink inwards from an initial radius of 0.12 pc (heavy lines) and from 0.17 pc (light lines) for stars of mass $2 M_{\odot}$ (continuous lines) and $4 M_{\odot}$ (short-dashed lines). In each case, we have assumed the usual velocity dispersion profile [Equation (2)] and two values of the density profile: that of Genzel *et al.* (1996) and the cusp-like profile (see §2.4); the former gives rise to a longer segregation time-scale and thus, for a given star, is always the higher line. The horizontal dotted lines indicate the lifetimes of $2 M_{\odot}$ stars (upper line) and $4 M_{\odot}$ stars (lower line).

whereas the latter is only present in the deep GC when at periastron. A segregated giant on an eccentric orbit will, of course, have more collisions than in the other two cases.

Assuming that all other stars were solar-type, from Equation (5) we calculate that a $4 M_{\odot}$ star indigenous to 0.02 pc would undergo ~ 80 collisions, and a $2 M_{\odot}$ star on a circular orbit at 0.01 pc would undergo ~ 400 collisions. Figure 10 shows that at such low radii, the time-scale for a $2 M_{\odot}$ giant to undergo a collision that leads to a common-envelope system is longer than the stellar lifetime; this is very likely also true for a $4 M_{\odot}$ giant. Thus the formation of bound systems cannot destroy enough of the giants to account for the paucity.

The mass lost from the envelope drops with increasing impact speed, and so collisions at very low galactocentric radii will involve lower mass losses than the (small) quantities reported in §6. Individually, therefore, solar mass impactors cannot destroy the giants, but it may be possible that the giants could be progressively stripped of their envelopes over the many collisions that they would suffer. Impacts of speeds germane to the very low-radius GC ($V_{\infty} \gtrsim 800$ km/s) with solar-mass impactors will only remove small amounts of envelope mass from either giant, and so it is unclear whether solar-mass impactors may be effective in destroying giants. Impactors of greater mass may be more effective. For a target giant in a sea comprised solely of $8 M_{\odot}$ impactors (black holes), the number of collisions will be reduced by a factor of eight compared to solar-type

impactors. Cumulative mass loss via several collisions may remove most of the giants' envelopes. Alternatively, if a giant is likely to undergo several collisions with very massive impactors, there may be a significant probability of a very low impact-parameter collision. This raises the possibility of the core being pulled out of the envelope by the massive impactor, thereby destroying the giant. An important problem with this high-mass impactor scenario is that $2 M_{\odot}$ stars generally cannot sink as far into the GC if the local mean mass increases from our assumed $1 M_{\odot}$ to $8 M_{\odot}$.

Collisions involving mass-segregating main-sequence stars may be important in the destruction of stars before they evolve into giants. Unlike the giant phase, the main-sequence stars will undergo collisions distributed over the range of radii through which the stars sink. For the main-sequence counterparts of the two giants considered above, the upper limit of the numbers collisions suffered is about 30 collisions for the $2 M_{\odot}$ star and about two collisions for the $4 M_{\odot}$ star, for solar-type impactors and assuming a cusp-like density profile. Collisions between main-sequence stars at the high speeds involved may lead to a significant amount of mass loss and possibly a merger of the two stars, depending on the impact parameter and mass ratio of the colliders (Benz & Hills 1987, 1992; Lai, Rasio & Shapiro 1993). It is quite possible that potential giants may be destroyed via mass loss in collisions whilst on the main-sequence, if the deep GC density profile is cusp-like. The merging of the two main-sequence stars into a higher-mass star has the effect of removing two potential lower-mass giants from the galactic centre whilst adding a higher-mass star that will eventually evolve into a massive giant. If such a process occurs, then it is inconsistent with the paucity observed by Genzel *et al.* (1996) because massive giants are extremely luminous whereas the observations show an absence of such stars in the deep GC.

Another consideration must be the process of *resonant dynamical friction* (see §9.3), which may take place deep in the GC. As the mass-segregation time-scale is similar to the relaxation time-scale, resonant dynamical friction may give rise to segregation time-scales shorter than the normal segregation time by a factor $\sim 7M_{\text{st}}/M_{\text{bh}}$ (see Rauch & Tremaine 1996), where M_{st} is the enclosed stellar mass inside a given radius. This process should not occur for a system in which the orbits are isotropic (Rauch & Tremaine 1996). In a spherically symmetric, well-mixed distribution of orbits, however, the density profile cannot decrease inwards. Obviously, the observed paucity of the brightest red giants means that the density distribution of those stars does decrease inwardly within the central ~ 0.2 pc, thereby implying that the brightest giants' orbits are not well-mixed or isotropic. However, resonant dynamical friction allows orbits to drift in angular momentum space, rather than in energy space and thus their semi-major axes would remain constant.

9.3 Tidal disruption by a central, massive black hole

The galactic centre likely harbours a $2 \times 10^6 M_{\odot}$ black hole (Eckart & Genzel 1997). Stars will be disrupted if they approach the black hole to within the tidal radius, which is given by (Hills 1975):

$$R_t = \left(\frac{6M_{\text{bh}}}{\pi\rho_1} \right)^{1/3} \quad (16)$$

where $M_{\text{bh}} = 2 \times 10^6 M_{\odot}$ and ρ_1 is the mean density of the star. We find that $R_t = 7.4 \times 10^{-4} \text{ pc} = 3 \times 10^5 R_{\odot}$ for a star of mass $8 M_{\odot}$ and radius $243 R_{\odot}$. For a giant of mass $2 M_{\odot}$ and radius $94 R_{\odot}$, $R_t = 4.6 \times 10^{-4} \text{ pc}$. In other words, if these giants had orbital semi-major axes of 0.1 pc, they would require eccentricities > 0.993 for them to be disrupted. Assuming isotropic orbits, the probability, P_t , of a star being on an orbit that takes it inside the tidal radius is given by (e.g. Sigurdsson & Rees 1997):

$$P_t \simeq \frac{R_t}{d} \quad (17)$$

where d is the semi-major axis of the star's orbit. For the star of mass $8 M_{\odot}$ and radius $243 R_{\odot}$, $P_t \sim 7 \times 10^{-3}$. The observed paucity of giants may be explained by tidal disruption only if, on time-scales shorter than the giants' lifetimes, the orbits of *all* the giants are scattered into the phase space occupied by the loss cone. The time-scale for such scattering to occur is usually taken to be the relaxation time [Equation (13)], but nearly Keplerian potentials (such as that near the central black hole) can allow faster *resonant relaxation* to occur (Rauch & Tremaine 1996). This process is important within the galactocentric radius at which $\mu_{\text{enc}} = M_{\text{st}}/(M_{\text{st}} + M_{\text{bh}}) = 0.1$ (Rauch & Ingalls 1998), where M_{st} is the total enclosed stellar mass. Within the region of missing bright giants ($\lesssim 0.2 \text{ pc}$), μ_{enc} satisfies this condition, assuming either the cusp-like density profile or that of Genzel *et al.* (1996) (see §2.4). The resonant relaxation time-scale is given by Rauch & Tremaine (1996):

$$\tau_{\text{res}} = \frac{7M_{\text{st}}}{M_{\text{bh}}} \tau_{\text{rel.}} \quad (18)$$

Well inside the region in which the bright giants are depleted, say at 0.1 pc, $\tau_{\text{res}} \sim 4 \times 10^8 \text{ years}$, assuming a mean stellar mass of $\sim 1 M_{\odot}$ and assuming the density profile of Genzel *et al.* 1996 (the cusp-like profile actually gives rise to longer resonant relaxation time-scales as the enclosed stellar mass is higher). Given the small size of P_t and also that the resonant relaxation time is longer than the giant phases of the stars (see Table 1), we conclude that tidal disruption via relaxation cannot account for the paucity.

Giants may also enter the loss cone via precession if the GC stellar distribution (and thus potential) were flattened from spherical, as the total angular momentum of a giant in such a potential is not conserved. If the flattening is along, say, the z -direction, then two of the star's angular momentum components (J_x and J_y) are not conserved whereas J_z is conserved. For giant stars on orbits of $d = 0.1 \text{ pc}$ to pass within R_t of the black hole, the required values of J_z represent only a small fraction of the full range available. Thus precession into the loss cone in a flattened asymmetric potential in the GC cannot account for the missing bright giants.

We conclude that tidal disruption cannot account for the paucity of the bright giant stars.

9.4 Binary stars

Interactions between binary stars and red giants in the GC were considered by Davies *et al.* (1998). Such interactions

can explain the observed paucity only if the giants are low mass ($2 M_{\odot}$ rather than $8 M_{\odot}$) and also if the stars can be hit at earlier stages of their evolution. A high binary fraction in the GC population is also required. If these conditions are satisfied then hard binaries will be more destructive towards giants than single stars. For stellar collisions to occur in a binary-single star encounter, one expects $R_{\text{min}} \lesssim d$. The collision rate for such encounters is less dependent on the individual size of the interacting stars than are two-body encounter rates. Thus main-sequence stars, which are smaller but longer lived than giants, will play a greater role in 2+1 body encounters than in single-single collisions. If a sufficient number of collisions occur in 2+1 body encounters then the *precursors* of the bright-giant stars may be destroyed before they ascend the giant branch. This will be investigated in future work.

For sufficiently tight binaries, the size of the primary's Roche lobe limits the primary's size, or may even lead to the premature end of the primary's evolution. The binary separation, d_{hs} , for which single cluster members have *just* enough kinetic energy to break up the binary is given by:

$$d_{\text{hs}} = \frac{GM_a M_b (M_a + M_b + M_c)}{M_c (M_a + M_b)} \frac{1}{V_{\infty}^2} \quad (19)$$

(e.g. Davies 1995) where V_{∞} is the relative velocity between the binary and the single star; M_a , M_b and M_c are respectively the masses of the two binary components and the mass of a third-body intruder. Deep in the GC, the mass of the central black hole dominates, forcing stars to follow Keplerian orbits (see Eckart & Genzel 1997). As the velocities and velocity dispersions of the stars are independent of their masses, the *relative* velocity dispersion between a binary ab and single star c is therefore $\sigma_{ab,c}^2 = \sigma_{ab}^2 + \sigma_c^2 = 2\sigma^2$ and the mean-square velocity is $\langle V_{\infty}^2 \rangle = 3\sigma_{ab,c}^2 = 6\sigma^2$. Substituting $\langle V_{\infty}^2 \rangle$ for V_{∞}^2 in Equation (19), we find for $\sigma(r)$ appropriate for the GC, d_{hs} is indeed small ($\lesssim 2 R_{\odot}$ for $M_a = M_b = M_c = 1 M_{\odot}$). The time-scale for two objects to pass within, say, $100 R_{\odot}$ of each other deep in the GC is $\sim 10^7 \text{ years}$. With the exception of the tightest binaries, most binaries will have been ionised before the primary could evolve off the main sequence. We therefore expect most of the GC giant stars to be single and so the observed paucity of bright giants cannot be explained in terms of giants' evolution being restricted in tight binaries. Another problem with this scenario is that it does not explain why the bright giants disappear rather precipitously at about 0.2 pc.

10 CONCLUSIONS

Our chief conclusions may be summarised as follows:

- (i) The mass losses that result from single-single stellar encounters involving red giants in the galactic centre are almost always low ($\lesssim 0.1 M_{\odot}$). Only a very small number of collisions will involve sufficient mass loss to destroy the giant. Such collisions require low R_{min} ($\lesssim 30 R_{\odot}$) and preferentially high-mass impactors ($\gtrsim 8 M_{\odot}$). Such high mass loss collisions are thus unlikely to account for the observed paucity of bright red giants.
- (ii) Mass loss was found to be an increasing function of impactor mass and decreasing functions of R_{min} and V_{∞}

reflecting that gravitational forces rather than shock mechanisms dominated the collisions.

(iii) Tidal capture of impactors by giant stars is unlikely to occur in the galactic centre. Most collisions involved the impactor passing through the giants and remaining unbound. This is due to the high velocity dispersion associated with the galactic centre.

(iv) The fraction of the impactor's orbital energy ($\Delta E/E$) deposited in the giant increased with impactor mass and decreased with increasing R_{\min} and V_{∞} . For sufficiently small R_{\min} and V_{∞} the impactor became bound to the giant, immediately forming a common envelope system or an eccentric binary system which would rapidly decay into a common envelope system. The fraction of collisions resulting in these bound systems was $\lesssim 0.5$ at a few pc, decreasing to $\sim 10^{-5}$ at very low radii, depending upon the impactor mass. At the radius at which the luminous giants are missing (~ 0.2 pc), the fraction was $\sim 10^{-2} - 10^{-3}$.

(v) We showed that many of these common envelope systems formed would lead to total envelope ejection for the $2 M_{\odot}$ giant and also for the $8 M_{\odot}$ giant if the efficiency was high or the impactor was a high-mass main-sequence star or a stellar remnant. However, even if all common envelope systems destroy the giant, the time-scale for collisions which result in these bound systems was at least the *entire* lifetimes of stars of masses $\gtrsim 2 M_{\odot}$ and so could not account for the paucity of the giants.

(vi) The time-scale for creating bound systems was only weakly dependent of the impactor mass and so can reveal little about the nature of the undetectable stellar population of the galactic centre.

(vii) Giants (or their precursors) within the GC *may* be destroyed in collisions involving high mass losses if their orbits are sufficiently eccentric to take the stars deeper into the galactic nucleus where the collision rate is higher. This requires, however, that we currently significantly underestimate the stellar density deep in the GC.

(viii) Dynamical friction and resonant dynamical friction may allow stars, originally on wide orbits at about 0.2 pc (the outer radius at which bright giants are observed to be missing), to travel deep into the galactic nucleus, thereby becoming subject to a greatly increased collision rate. This study does not rule out the possibility of the bright giants (or their precursors) being destroyed in such collisions. This process is only significant, however, if the galactic-centre has a cusp-like density profile, rather than the observed flattened profile.

(ix) The absence of the giant stars is not due to tidal disruption around a central black hole of mass $2.5 \times 10^6 M_{\odot}$, nor does it seem likely to be due to single-single stellar collisions involving giants. To explain the paucity in terms of stellar collisions requires investigation into the collisional effects of binary stars upon pre-giant stars. Hard binaries in the galactic centre may well have separations too small for the primary to evolve into a giant. This also, however, means that most binaries will have been ionised and so most giants will be single stars (unless, perhaps, they exchange into a binary). It also does not seem to explain why the numbers of bright giants plummet rapidly at ~ 0.2 pc.

ACKNOWLEDGEMENTS

We thank J. Brinchmann, P. Eggleton, J. Hurley, J. Magorrian, S. Sigurdsson and C. Tout, of the IoA and R. Genzel (MPE-Garching) for valuable discussions. We also thank the referee for insightful comments. Simulations were performed at T6 (Los Alamos National laboratory) and at the IoA; we are grateful to M. Warren & M.P. Goda (T6, LANL) for technical support. This work was supported through an IGPP research grant at Los Alamos. VCB was supported by a PPARC grant. MBD gratefully acknowledges the support of a URF from the Royal Society.

REFERENCES

Binney J.J., Tremaine S., 1987, *Galactic Dynamics*. Princeton
 Bahcall J.N., Wolf R.A., 1976, *ApJ*, 209, 214
 Benz W., 1990, *The Numerical Modelling of Nonlinear Stellar Pulsations*, J.R. Buchler (ed.), 269
 Benz W., Hills J.G., 1987, *ApJ*, 323, 614
 Benz W., Hills J.G., 1992, *ApJ*, 389, 546
 Blum R.D., Sellgren K., DePoy D.L., 1996, *ApJ*, 470, 864
 Davies M.B., 1995, *MNRAS*, 276, 887
 Davies M.B., Benz W., Hills J.G., 1991, *ApJ*, 381, 449
 Davies M.B., Benz W., Hills J.G., 1992, *ApJ*, 401, 246
 Davies M.B., Blackwell R., Bailey V.C., Sigurdsson S., 1998, *MNRAS*, 301, 745
 de Kool M., 1990, *ApJ*, 358, 189
 Eckart A., Genzel R., 1997, *MNRAS*, 284, 576
 Eckart A., Genzel R., Hofmann R., Sams B.J., Tacconi-Garman L.E., 1995, *ApJ*, 445, L23
 Eggleton P.P., 1983, *ApJ*, 268, 368
 Genzel R., Hollenbach D., Townes C.H., 1994, *Rep. Prog. Phys.* 57, 417
 Genzel R., Thatte N., Krabbe A., Kroker H., Tacconi-Garman L.E., 1996, *ApJ*, 472, 153
 Han Z., Podsiadlowski P., Eggleton P.P., 1994, *MNRAS*, 270, 121
 Hills J.G., 1975, *Nat*, 254, 295
 Hut P., McMillan S., Romani R., 1992, *ApJ*, 389, 527
 Johnson H.L., 1966 *ARA&A*, 4, 193
 Morris M., 1993, *ApJ*, 408, 496
 Pols O.R., Schroder K.-P., Hurley J.R., Tout C.A., Eggleton P.P., 1999, in prep
 Pols O.R., Tout C.A., Eggleton P.P., Han Z., 1995, *MNRAS*, 274, 964
 Rauch K.P., Ingals B., 1998, *MNRAS*, 299, 1231
 Rauch K.P., Tremaine S., 1996, *New Astron.*, 1, 149 (RT96)
 Quinlan G.D., Hernquist L., Sigurdsson S., 1995, *ApJ*, 440, 554
 Rasio F.A., Shapiro S.L., 1991, *ApJ*, 377, 559
 Rieke G.H., Rieke M.J., Paul A.E., 1989, *ApJ*, 336, 623
 Saha P., Biknell V., McGregor P.J., 1996, *ApJ*, 467, 636
 Sandquist E.L., Taam R.E., Chen X., Bodenheimer P., Burkert A., 1998, *ApJ*, 500, 909
 Sigurdsson S., Rees M., 1997, *MNRAS*, 284, 318
 Taam R.E., Bodenheimer P., 1989, *ApJ*, 337, 849
 Tout C., Pols O.R., Eggleton P.P., Han Z., 1996, *MNRAS*, 281, 257